

Radio-Frequency-Transparent, Electrically Conductive Graphene Nanoribbon Thin Films as Deicing Heating Layers

Vladimir Volman,^{*,†,‡} Yu Zhu,^{§,‡} Abdul-Rahman O. Raji,[§] Bostjan Genorio,[§] Wei Lu,[§] Changsheng Xiang,[§] Carter Kittrell,[⊥] and James M. Tour^{*,§,⊥,||}

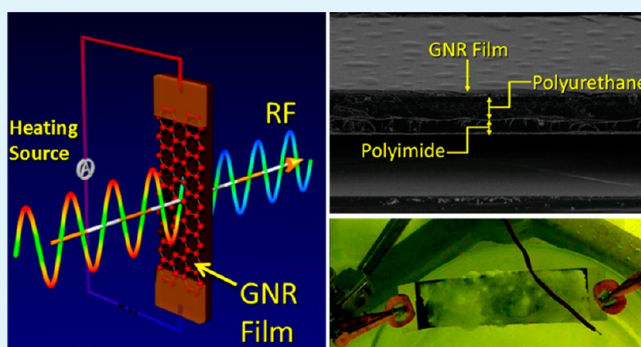
[†]Lockheed Martin Corp., MS2, Mail Stop 137-101, 199 Borton Landing Road, Moorestown, New Jersey 08057-0927, United States

[§]Department of Chemistry, [⊥]Richard E. Smalley Institute for Nanoscale Science and Technology, and ^{||}Department of Mechanical Engineering and Materials Science, Rice University, 6100 Main Street, Houston, Texas 77005, United States

Supporting Information

ABSTRACT: Deicing heating layers are frequently used in covers of large radio-frequency (RF) equipment, such as radar, to remove ice that could damage the structures or make them unstable. Typically, the deicers are made using a metal framework and inorganic insulator; commercial resistive heating materials are often nontransparent to RF waves. The preparation of a sub-skin-depth thin film, whose thickness is very small relative to the RF skin (or penetration) depth, is the key to minimizing the RF absorption. The skin depth of typical metals is on the order of a micrometer at the gigahertz frequency range. As a result, it is very difficult for conventional conductive materials (such as metals) to form large-area sub-skin-depth films. In this report, we disclose a new deicing heating layer composite made using graphene nanoribbons (GNRs). We demonstrate that the GNR film is thin enough to permit RF transmission. This metal-free, ultralight, robust, and scalable graphene-based RF-transparent conductive coating could significantly reduce the size and cost of deicing coatings for RF equipment covers. This is important in many aviation and marine applications. This is a demonstration of the efficacy and applicability of GNRs to afford performances unattainable by conventional materials.

KEYWORDS: graphene nanoribbon (GNR), radio-frequency (RF) transparent, electrically conductive film, carbon-based thin film, deicing, radome, radar, transmission loss, skin effect



INTRODUCTION

Ice-elimination systems are very common in large radio-frequency (RF) structures. They can be classified as either passive antiicing films (preventing the accumulation of ice) or active deicing devices (removing ice after accumulation). A typical application of an icing protection system is in radomes. Radomes are protecting shells or covers for radar instruments in aviation and marine environments. The radomes are subject to hostile environments, such as high winds containing sand, rain, hailstones, and saltwater, over wide temperature variations. Explosive pressure blasts can also take place nearby the radomes. Thus, radome deicing conductive films must be extremely tough with good adhesiveness to the heated surface. In addition, these deicing structures must not compromise the reliability of the original RF system, which, in the case of radome applications, means that the deicing film must be predominately transparent to RF radiation at any polarization with minimal impact on the antenna scan performance. It is desirable that this film be lightweight and low-cost, with physical characteristics that allow it to cover large curved surface areas. Currently, most radome systems are constructed

using a metal wire framework with supporting ceramic materials.^{1–3} The metal wire framework serves as the conductive layer, and the ceramic materials are the heat transfer medium. Because of the strong RF absorbance of metals, they need to be installed far from the RF source to achieve minimal RF attenuation. Consequently, current radomes are large, heavy, and costly, complicating their use on aircraft and ships.

The RF signals propagating through a material can be attenuated by absorption, reflection, or scattering.⁴ Randomly dispersed multilayer graphene nanoribbons (GNRs) form isotropic or very close to isotropic conductive films. Each multilayer GNR component of the film is made of several crystallographically stacked narrow graphene monolayers that are 0.3 nm thick.^{5–9} Because 1 nm = 10⁻⁶ mm, a film of 100 nm thickness is a tiny fraction of wavelength even for RF signals up to 300 GHz (1 mm wavelength). We can evaluate the

Received: September 25, 2013

Accepted: December 11, 2013

67 propagation through such films using the classical skin effect
68 concept¹⁰ where the electrical field strength E (V/m) in the
69 conductive layer decreases exponentially from its value at the
70 surface, as in eq 1.

$$71 \quad E \sim E_0 e^{-d/\Delta} \quad (1)$$

72 where d is the film thickness in meters and Δ is the distance at
73 which incident E (i.e., E_0) diminishes to $1/e$ or $\sim 37\%$ of its
74 original value (a detailed discussion of eq 1 is included in the
75 Supporting Information). On the basis of this equation, the
76 electrical field strength can be very small with an ultrathin
77 conductive film (where $d \ll \Delta$). Because the GNR film is
78 ultrathin, the electrical field variation is small and the
79 electromagnetic waves reflected from the front and back
80 surfaces of the film cancel each other because they are
81 practically equal in magnitude and opposite in phase. Thus, we
82 can expect a very low mismatch loss that is nearly insensitive to
83 frequency. Then according to eq 2, the film full transmission
84 loss L in decibels is defined by the frequency, the physical
85 thickness of the film, and the conductivity of the film.

$$86 \quad L = -126d\sqrt{f\sigma} \quad (2)$$

87 Here we disclose a new radome deicing coating based on an
88 ultrathin conductive GNR film. A high-throughput spray-
89 coating technique was developed to prepare GNR films that
90 can function as the conductive layer for deicing coatings of
91 large RF equipment such as bridge antenna towers and radome
92 systems. In the new deicing system, the ultrathin GNR layer is
93 used to conduct direct current (dc) or alternating current. The
94 resistance of the GNR film is adjustable and is enough to
95 generate sufficient heat for deicing the protected surface at
96 voltages that are commonly used aboard ships and aircraft. The
97 conductive GNR film is demonstrated to be thin enough to be
98 transparent to RF signals. We have further demonstrated that
99 ice formation on the protected surface can be prevented while
100 the antenna array is operational.

101 ■ EXPERIMENTAL METHODS

102 **GNR Film Preparation.** GNRs were synthesized based on
103 previous reports.^{11,12} GNRs were suspended in *o*-dichlorobenzene
104 (ODCB) at a concentration of 1 mg/mL and bath-sonicated (12 W;
105 model 08849-00, Cole-Parmer) immediately before use. The
106 polyimide film (McMaster, 25 μm thickness) was cleaned with
107 acetone and deionized water and dried. Polyurethane (clear-coat
108 Dupli-Color auto paint, O'Reilly Auto Parts) was spray-coated on the
109 polyimide substrate and dried at room temperature for 24 h. The
110 polyurethane-coated polyimide substrate was placed atop a hot plate at
111 220 $^\circ\text{C}$, and the GNR solution was spray-coated on the substrate using
112 an Iwata airbrush connected to compressed nitrogen. The composite
113 film was removed from the hot plate immediately after the spraying.

114 **Waveguide Test and Simulation.** A waveguide kit (WR-284)
115 was first calibrated between 2.1 and 4 GHz. The sample was then
116 mounted into the waveguide, and S_{11} and S_{21} were measured in series.
117 The transmission coefficient in decibels is $10\log$ (transmitted power/
118 incident power). The transmission loss in decibels is $-10\log$
119 (transmitted power/incident power) or $-$ transmission coefficient.
120 The waveguide simulation was carried out by using Ansoft's high-
121 frequency structure simulator (HFSS) 14.0.

122 **Characterization.** Scanning electron microscopy (SEM) images
123 were taken using a JEOL 6500 scanning electron microscope and a
124 FEI Quanta 400 field-emission gun scanning electron microscope.
125 Transmission electron microscopy (TEM) images were taken using a
126 200 kV JEM 2100F microscope.

■ RESULTS AND DISCUSSION

127

Materials and Ultrathin GNR Film Preparation. The
128 high-aspect-ratio, nonoxidized GNRs were synthesized by
129 splitting multiwalled carbon nanotubes (MWCNTs) with
130 potassium vapor or a sodium–potassium alloy.^{11–13} The raw
131 materials, MWCNTs, are much less expensive than single-
132 walled carbon nanotubes. Over 500 tons/year of MWCNTs are
133 produced. In one chemical step, MWCNTs are converted to
134 GNRs, and the process is scalable. The produced GNRs (the
135 TEM images of single GNRs used in this work are shown in
136 Figure S1 in the Supporting Information) are free of oxidation
137 and relatively conductive. In addition, they are solution-
138 processable and compatible with many thin-film formation
139 techniques such as spray, spin, or blade coating. Compared to
140 graphene oxide, the GNRs are more promising materials for
141 thin conductive film coatings because they need no annealing
142 to achieve the high-conductivity state. The single GNRs exhibit
143 conductivities over 60000 S/m.^{11,12} The electrical conduction
144 mechanism through the GNRs is the same as that through bulk
145 graphite, as we have described in our previous work,^{11,12} where
146 detailed electrical measurements of the GNRs were performed.
147 A significant difference between GNRs and bulk graphite is that
148 it is much easier to attain an electrically percolative network
149 with GNRs because of their high aspect ratio, thus facilitating
150 the fabrication of conductive thin films. In comparison to other
151 carbon materials, conventional carbon black has much lower
152 conductivity compared to the GNRs. As a result, it requires
153 much higher voltage to deliver the same amount of heat for the
154 same size sample. It is thus not practical to use carbon black for
155 resistive heating on equipment such as radomes. Although
156 MWCNTs have conductivity similar to that of GNRs, the films
157 produced from them would be thicker and would not meet the
158 ultrathin film requirement for RF transparency because of their
159 tubular structure. Functionalizing the sidewalls of nanotubes for
160 dispersion in a solvent would make them less conductive
161 compared to the GNRs, where only the edges are function-
162 alized for enhanced dispersion. We have developed GNR-based
163 thin films that were produced using large-area coating
164 techniques such as spray coating.^{14,15} Our previous work
165 demonstrated that GNRs can be dispersed in ODCB at
166 concentrations up to ~ 1 mg/mL.¹¹ Here, the GNRs were
167 synthesized based on the reported work and dispersed in
168 ODCB, and the dispersion was used in a high-throughput
169 spray-coating procedure for preparing thin GNR films on
170 polymer substrates.

171 GNR films with various thicknesses and sheet resistances
172 were prepared (see the Experimental Methods for details).
173 Polyimide was used as the substrate in this work because it is
174 resistant to the ODCB solvent and stable to >200 $^\circ\text{C}$. In the
175 initial test, it was found that the GNR films did not adhere well
176 to the polyimide substrate. Thus, commercially available clear-
177 coat Dupli-Color automotive paint (pigment- and dye-free
178 polyurethane, which adheres well to the substrate) was used as
179 an adhesive layer in which the GNRs could be embedded. The
180 polyurethane (~ 30 nm thick) was spray-coated on the
181 polyimide and permitted to dry. Polyurethane was found to
182 be a robust protective coating that works well in our
183 experiments. The polyimide–polyurethane film was then
184 placed on a 200 $^\circ\text{C}$ hot plate in a fume hood. The ODCB
185 suspension of the GNRs was then spray-coated atop the
186 polyurethane, whereupon ODCB rapidly evaporated, leaving
187 the GNRs well-embedded in the polyurethane adhesion layer.
188

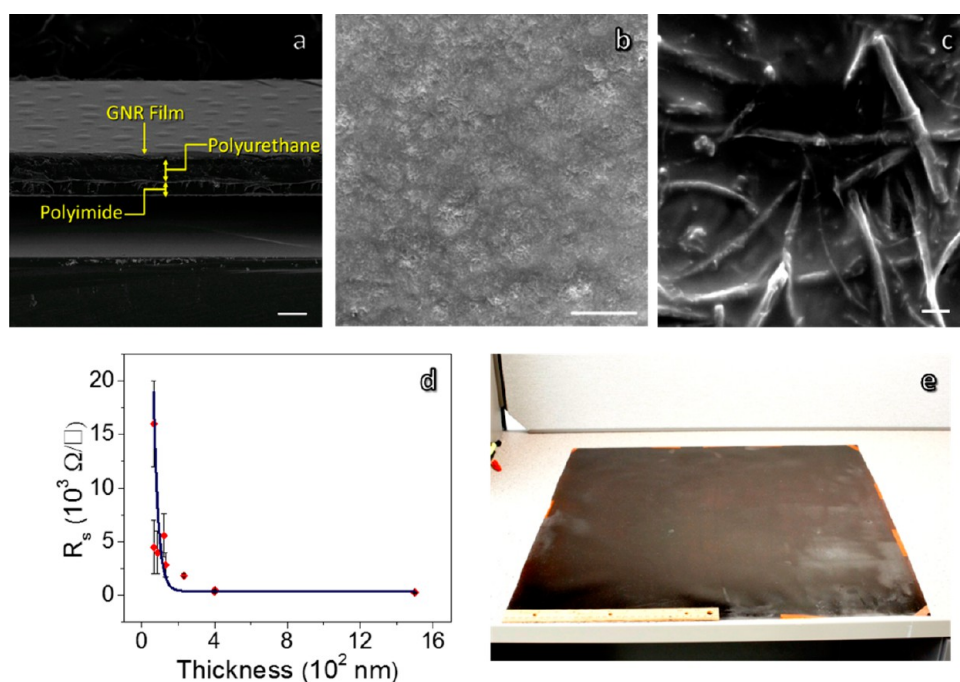


Figure 1. Characterization of ultrathin GNR films. (a) SEM cross-sectional image of the ultrathin GNR film. The bottom layer is the polyimide substrate ($25\ \mu\text{m}$ thick). The middle is the clear-coat Dupli-Color automotive paint (pigment- and dye-free polyurethane). The upper layer is the GNR film, which is also embedded in the polyurethane layer. Scale bar = $100\ \mu\text{m}$. (b) Top view of the SEM image of the GNR film that shows GNRs embedded in the polyurethane. Scale bar = $100\ \mu\text{m}$. (c) High-resolution SEM image of the GNR film. The GNRs are entangled to form a conducting percolated network embedded in polyurethane. The center dark rectangular region was formed while focusing the instrument because of the charging effect of the polymer substrate. Scale bar = $1\ \mu\text{m}$. (d) Relationship of the GNR film thickness and sheet resistance. The sheet resistance was determined by the four-point probe method. (e) A $0.6 \times 0.6\ \text{m}^2$ ($2 \times 2\ \text{ft}^2$) GNR film on polyimide. This sample was prepared in the laboratory using the spray-coating technique and a commercially available air brush. The large film was heated using three heating plates covered with a $1.3\ \text{cm}$ ($0.5\ \text{in}$) thick panel of aluminum. A $30.5\ \text{cm}$ ($1\ \text{ft}$) ruler is in the lower left.

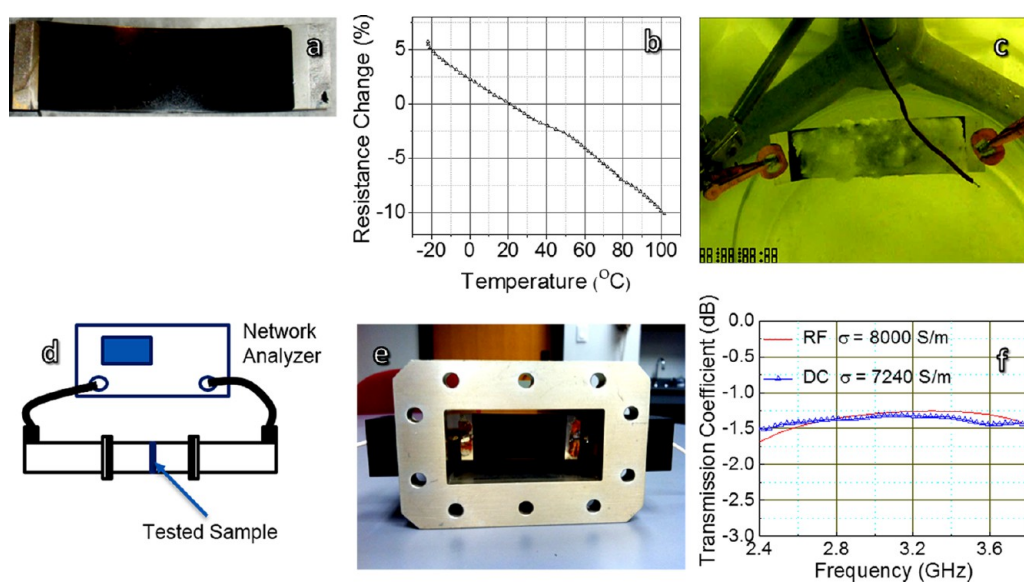


Figure 2. Deicing and transmittance tests. (a) Polyimide/polyurethane/GNR sample with platinum coated at the two ends. The size of the active GNR film (the center black region) is $25.4 \times 76.2\ \text{mm}^2$. (b) GNR film resistance change over a temperature range. (c) Picture from the video of the deicing demonstration at $-20\ ^\circ\text{C}$. The GNR film is connected to two flat copper clamps that are connected to the power source. The ice is preformed on the surface of the GNR film. The wire hanging above the GNR film is a thermocouple to monitor the environmental temperature, which is maintained at $-20\ ^\circ\text{C}$ within the experimental observation box. With the current passing through the film, the ice is melted in minutes (see the Supporting Information for the full video). (d) Block diagram of the RF test assembly. The sample is mounted between two waveguides, and the RF wave was generated and analyzed by a network analyzer. The sample can be rotated in order to acquire the transmission coefficient at different angles. (e) WR-284 waveguide with the wired GNR film. (f) Transmission coefficient in decibels versus frequency for a GNR-coated polyimide film: comparison of HFSS simulated and experimental data. The red line is based on the HFSS simulation with a GNR film of $8\ \text{kS/m}$ RF conductivity and $110\ \text{nm}$ thickness. The blue line is the RF measurement of a 110-nm -thick GNR polyimide film with $7.24\ \text{kS/m}$ dc conductivity.

Table 1. Properties of GNR Films on a Polyimide Substrate Used for dc and RF Measurements^a

	R_s (k Ω / \square)	R (k Ω)	dc conductivity (kS/m)	approximate GNR film thickness (nm)	sample size (width \times length, mm)	V (V)	I (mA)	calculated energy delivered (W)
1	1.02	3.06	5.77	170	25.4 \times 76.2	151.5	49.5	7.5
2	1.92	5.76	5.21	100	25.4 \times 76.2	207.8	36.1	7.5
3	4.85	14.56	2.58	80	25.4 \times 76.2	330.0	22.7	7.5
4	1.26	2.51	7.24	110	25.4 \times 50.8			
5	4.97	9.94	2.68	75	25.4 \times 50.8			

^a R_s is the sheet resistance measured by a four-point probe. R is the dc resistance of the active GNR film. R_s values are lower than R values of films because they were measured for a smaller area. The GNR film thickness was estimated based on Figure 1d. The dc conductivity was calculated based on the resistance and the thickness. V and I are the applied voltage and current, during deicing, respectively. Films 4 and 5 are smaller because they needed to fit into a waveguide. This is the reason for the opposite trend between the sheet and dc resistance between samples 1 and 4 and samples 3 and 5.

Parts a–c of Figure 1 show the SEM images of ultrathin GNR films on flexible polyimide substrates. The GNRs were embedded throughout the adhesive polyurethane layer to form a network that is conductive through percolation. This composite film is very robust, and removal requires sandpaper treatment. The GNRs are not removable by touch or by pulling on the surface with adhesive tape. Through control of the spraying time or GNR solution concentrations, the thickness of the GNR films can be tuned to modulate the resistance of the films. The sheet resistance versus GNR film thickness was studied, and the results are shown in Figure 1d. Large samples, such as the GNR film panel measuring $0.6 \times 0.6 \text{ m}^2$ ($2 \times 2 \text{ ft}^2$) in Figure 1e, were prepared in the laboratory.

Design of GNR Films for Radome Deicing Coatings.

The dc conductivity was calculated through the measured resistance, as shown in eq 3:

$$\sigma = \frac{l}{AR} \quad (3)$$

where $A = wt$, in which A is the GNR layer cross-sectional area (nm^2), w is the GNR layer width (nm), t is GNR layer thickness (nm), l is the GNR layer length (nm), and R is the resistance (k Ω).

In order to melt ice on the surface, a heating power density of $\sim 0.386 \text{ W/cm}^2$ (2.5 W/in^2) is used because this is a common ship-board power-delivery quantity. As for the test, small samples (Figure S2 in the Supporting Information) were prepared. The two ends of the sample were sputter-coated with platinum as the electrodes, and the size of the active GNR film was $25.4 \times 76.2 \text{ mm}^2$ ($1 \times 3 \text{ in.}^2$; Figure 2a and Table 1, entries 1–3). The parameters of the samples are presented in Table 1 (entries 1–3). The voltage and current required to deliver the power were calculated based on Ohm's law. The results show that the voltage and current are within the applicable range of a common ship or aircraft power supply.

For practical applications, it is important to know how the GNR film responds to temperature variations. The results of thermal tests are shown in Figure 2b. The experimental setup to determine the temperature-dependent resistance of GNR films is shown in Figure S3 in the Supporting Information. According to the data, the GNR film has a negative temperature coefficient, which affords a much narrower range of temperature dependence than that found in typical metals such as copper, aluminum, or silver. The variation of the resistance is -10% from 20 to 100 $^\circ\text{C}$, significantly smaller than those for metals (typically $+30\%$ from 20 to 100 $^\circ\text{C}$). The smaller resistance change to the temperature is very helpful for these

applications. Thus, the GNR film delivers more reliable power from a stabilized voltage supply across any temperature range.

To demonstrate that the GNR film can meet the heat power requirements, the GNR film on polyimide shown in Figure 2a was put at a 45° angle with 5 g of ice that was grown atop the film. The ice had been grown by placing the polyimide/polyurethane/GNR film on a block of dry ice and spraying it with water from a mist bottle until the film accumulated 5 g of ice. A fan blowing over the dry ice provided a -20°C atmosphere in an insulated box to simulate freezing conditions, as recorded by the thermocouple above the film sample (Figure 2c). The dc power supply was connected to film electrodes, as shown in Figure 2c. After 3 min, the ice was completely removed from the area around the center of the GNR film; it took another 2.5 min to melt the ice close to the electrodes (Figure S4 in the Supporting Information).

RF Conductivity Measurements. It well-known that the bulk conductors such as silver, gold, or copper have similar dc and RF (in the gigahertz frequency range) conductivities.¹⁶ Prior published work concerning graphene RF conductance was focused on measurements of few-layered graphene, where the RF conductance of few-layered graphene slightly increases with the frequency; at 4 GHz, it is ~ 1.5 times higher than the dc conductance.¹⁷ Thus, classical skin-depth theory does not hold. However, the GNR films of $\sim 100 \text{ nm}$ thickness that are made of electrically percolating, long GNRs are structurally distinct from a few-layered, continuous sheet of graphene. Therefore, it is necessary to explore the actual RF conductivity of the GNR thin film that is much thinner than the skin depth. It is also important to determine the correlation between the dc and RF conductivity to assess the applicability of normal classical skin-depth theory in order to verify the equations introduced earlier for this specific system.

In this work, an S-matrix measurement waveguide technique was used to experimentally determine the RF conductivity. A GNR film with 110 nm thickness was prepared and the dc conductivity was measured to be 7240 S/m (entry 4 in Table 1). The film was fitted in the perpendicular position within a rectangular waveguide and was measured using a Vector Network Analyzer (Figure 2d). Figure 2e shows the GNR film mounted within the S-band WR-284 rectangular waveguide (to fit the size of the waveguide, the sample size was decreased to $25.4 \times 50.8 \text{ mm}^2$). Because the WR-284 waveguide cutoff frequency of the dominant mode is 2.08 GHz and the first high mode starts propagation at 4.16 GHz, all of the measurements were taken between 2.4 GHz (far enough from the dominant mode cutoff frequency to achieve low empty waveguide transmission loss) and 4 GHz (to be sure of a negligible level of high modes). The scattering parameters such as the

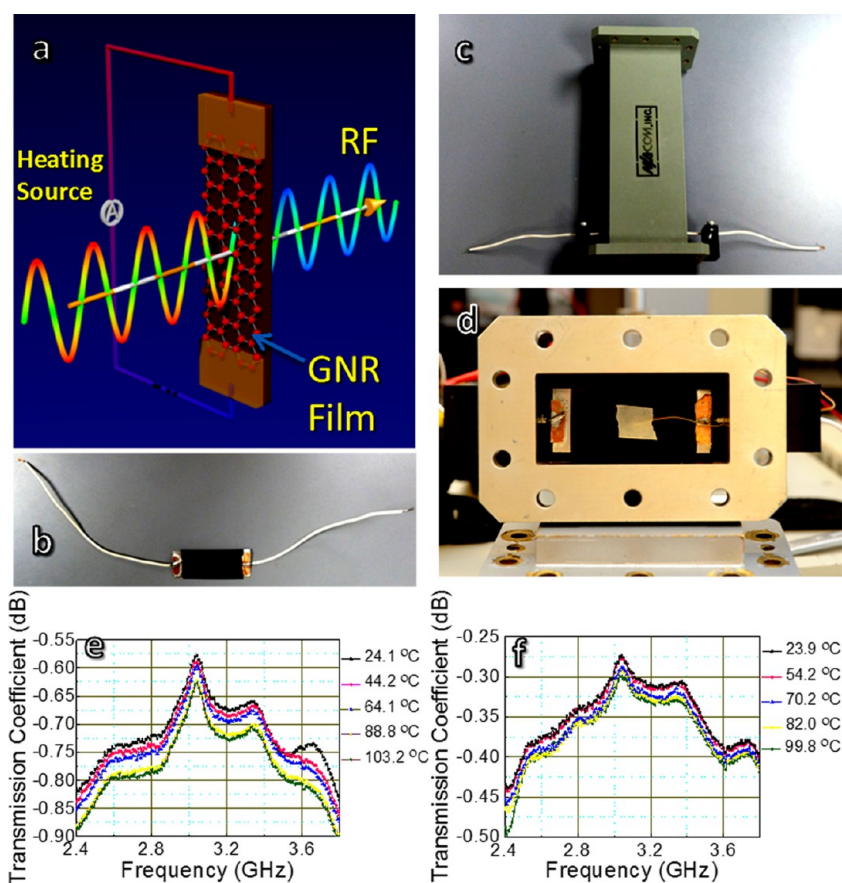


Figure 3. Real-time waveguide transmission test results. (a) Scheme of the real-time waveguide transmission test. The current passes through the GNR film during the RF measurement. This is to simulate the RF signal transmission when the deicing is progressing. (b) Wired GNR films. (c) Overview of the waveguide with the wired GNR film installed. (d) WR-284 waveguide with the wired GNR film. The thermal sensor is under the white tape patch covering the sensor, and it monitors the surface temperature of the GNR film. (e) Real-time waveguide transmission coefficient of the GNR film with a thickness of 110 nm (entry 4 in Table 1). (f) Real-time waveguide transmission coefficient of the GNR films with a thickness of 75 nm (entry 5 in Table 1). The legend on the right in parts e and f is the surface temperature of the GNR layer.

283 reflection (S_{11}) and transmission (S_{21}) of the waveguide section
 284 with and without GNR film samples were collected. Then the
 285 measured data (blue line in Figure 2f) were compared with the
 286 simulated transmission coefficient from Ansoft's HFSS to
 287 determine the RF conductivity. The details of the HFSS
 288 simulation are described in Figure S5 in the Supporting
 289 Information. The exact HFSS model of the same GNR film on
 290 a substrate was simulated with several RF conductivity values
 291 close to the dc conductivity value of the film. It was found that
 292 the best match between the measured and simulated data took
 293 place if the HFSS model of the GNR film had a RF conductivity
 294 of 8000 S/m (red line in Figure 2f). The ~9% difference
 295 between the dc and RF conductivities was expected and is
 296 predominantly related to a mismatch loss. The measured
 297 reflection coefficient from the GNR film alone, with no
 298 electrodes, is below -20 dB. The reflection of electromagnetic
 299 waves from the GNR layer can be calculated as the
 300 superposition of all electromagnetic waves reflected at the
 301 front and back boundaries between areas of different dielectric
 302 properties. Because of the extremely small GNR film thickness
 303 in comparison to the wavelength at S-band frequencies, most of
 304 these reflected waves cancel each other. Additional GNR films
 305 were tested, and the RF sheet resistance values are plotted with
 306 dc sheet resistance values in Figure S6 in the Supporting
 307 Information. In all cases, a very good correlation between the
 308 dc and RF conductivities was demonstrated. A good match

between HFSS simulations based on normal classical skin- 309
 depth theory and the experimental waveguide tests shows that 310
 conventional conductive material concepts hold for the GNR 311
 films. 312

Real-Time Waveguide Transmission Test. The real-time 313
 waveguide transmission test scheme is shown in Figure 3a. The 314
 setup is shown in Figure 3b–d. A two-port network analyzer 315
 was calibrated without a GNR film inside the waveguide 316
 between 2.4 and 3.8 GHz, and it provides a measurement of the 317
 complex transmission and reflection coefficients S_{ij} of the S 318
 matrix in eq 4: 319

$$\mathbf{S} = \begin{bmatrix} S_{11} & S_{12} \\ S_{21} & S_{22} \end{bmatrix} \quad (4) \quad 320$$

In Figure 3d, the two wide copper electrodes plated on the 321
 GNR layer are parallel to the vector of the electrical field in the 322
 waveguide, which formed an inductance diaphragm and served 323
 as a source of additional reflections. Therefore, an additional 324
 test was carried out to determine the reflection from the 325
 diaphragm only. The transmission coefficient of the GNR layer 326
 was calculated as the difference between the transmission 327
 coefficient of the GNR layer plus electrodes and the 328
 transmission coefficient of the electrodes only. The results of 329
 these measurements are shown in Figure 3e,f. 330

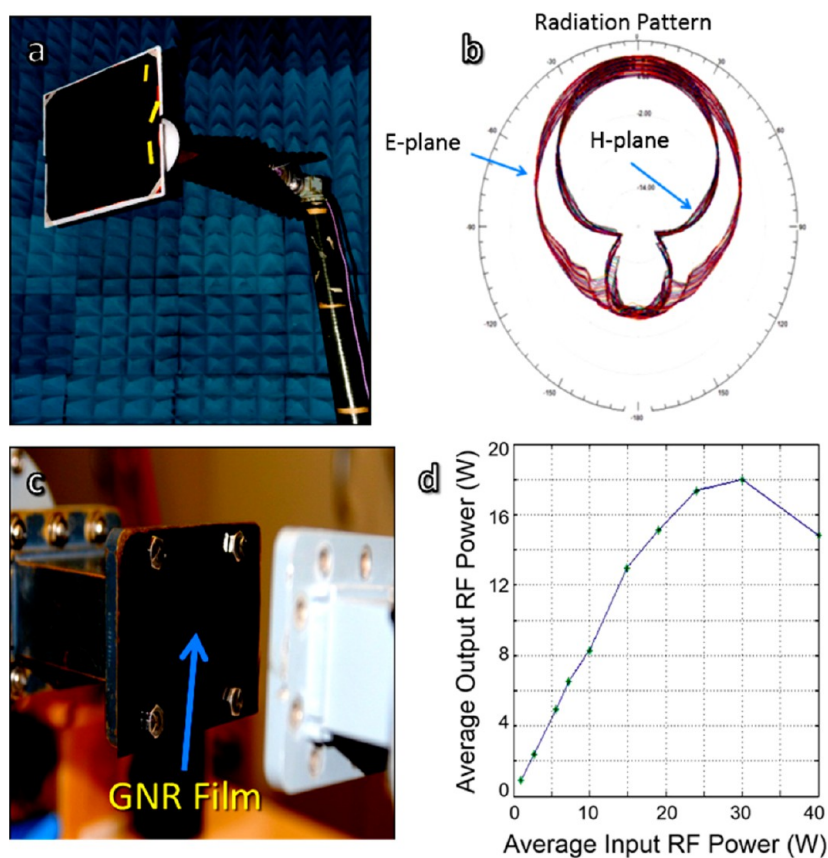


Figure 4. Antenna range test and high-power test results. (a) A $0.6 \times 0.6 \text{ m}^2$ ($2 \times 2 \text{ ft}^2$) GNR film in front of an open waveguide for the antenna range test. (b) HFSS-simulated radiation pattern of an open waveguide with a GNR film in front. The angles are labeled in 30° clockwise increments from 0° at the top to 150° , -180° at the bottom, and from -150° to -30° . (c) GNR film window in a WR-284 waveguide for the high-power test. (d) Plot of the average output power versus input power. The linear region is up to 25 W in this specific case. The nonlinear behavior after 25 W is probably due to carbonization of the polymer substrate.

331 During the real-time waveguide transmission test, the voltage
 332 was applied to the GNR films to simulate the deicing working
 333 status. The RF transmission experiment was carried out
 334 simultaneously. As the current passes through the GNR films,
 335 the films become hot, and the surface temperature of the film
 336 was recorded by a flat thermocouple. The transmission loss
 337 decreases as the layer temperature increases (i.e., RF trans-
 338 mission decreases with temperature; Figure 3e,f). Thus, the RF
 339 transmission has the same negative temperature coefficient as
 340 the dc resistance. As expected, the GNR film behaves as a
 341 classical conductor with respect to the electromagnetic wave
 342 despite its negative temperature coefficient of resistance. Even
 343 though the loss slightly increases with temperature, it is still
 344 small because the material is much thinner than the skin depth.
 345 According to the results in Figure 3e,f, the transmission loss of
 346 a GNR film depends on the thickness and conductivity of the
 347 layer. For the GNR sample with a thickness of $\sim 110 \text{ nm}$, the
 348 transmission loss did not exceed 0.9 dB in the range of 2.4 to
 349 3.8 GHz. The sample of 75 nm thickness exhibited a better loss
 350 of $< 0.5 \text{ dB}$. The testing results convincingly suggest that the
 351 GNR films can replace the conventional deicing heat circuits,
 352 thereby improving the radome performance.

353 **Antenna Range Test and High Power Test.** Advanced
 354 modern radars are highly sophisticated systems with well-
 355 designed radomes that not only protect the enclosed radar
 356 antenna from harsh environments such as ice or freezing rain
 357 but also have a low impact on the electrical performance of the

358 antenna. Therefore, we must be sure that the additional GNR
 359 deicing layer on top of the radome does not lead to antenna
 360 system degradation such as significant gain reduction, side-lobe
 361 increase, depolarization, antenna beam steering, and broad-
 362 band performance. The objectives of the antenna range test
 363 described below were to verify the GNR film's high-RF
 364 transparency for any incident wave within the angular sector
 365 $\pm 60^\circ$ in wide-frequency bands.

366 A large $0.6 \times 0.6 \text{ m}^2$ ($2 \times 2 \text{ ft}^2$) GNR film for an antenna
 367 range test was prepared on a flexible polyimide substrate
 368 (Figure 1e). Figure 4a shows the large GNR film that was
 369 affixed in front of an open WR-284 rectangular waveguide to
 370 check the impact of the film on this simple antenna gain, cross-
 371 polarization performance, and shape of its pattern diagram.
 372 Because the return loss of this film measured in the waveguide
 373 was below -20 dB , the main reduction in the peak gain was
 374 related to the transmission loss (Figure 4b). The transmission
 375 loss was in the range of 0.2–0.4 dB at a frequency band of 2.6–
 376 4.0 GHz for any polarization in the angular sector $\pm 60^\circ$. No
 377 depolarization effect was detected. The testing results are in
 378 good agreement with the HFSS model based on classical skin-
 379 depth analysis, which is shown in Figure 4b.

380 The high-power tests were carried out in waveguide WR-284
 381 with the GNR film located between two waveguide flanges, as
 382 shown in Figure 4c. The typical dependence of the average
 383 output power versus average input power is shown in Figure
 384 4d. The linear characteristic behavior of input and output

385 power is up to 25 W (power density of about 20 kW/m²),
386 which is quite good for most antenna applications. The
387 nonlinear behavior was observed when the power was further
388 increased (in the sample shown in Figure 4d, >25 W). One
389 possible explanation, based on this test, is that the RF-
390 transparent GNR film did absorb a small amount of RF energy
391 that heated the polyurethane and polyimide substrates of the
392 film, leading to a change of the film morphology or
393 carbonization in the extreme case. However, it should be
394 emphasized that the power density of ~20 kW/m² already
395 meets most antenna application specifications, and further
396 improvement in the substrate materials could enhance the high-
397 power test performance. We conjecture that there are local
398 regions of thicker GNR film thickness because of puddling
399 during spray coating of the GNRs onto the wavy polyimide
400 film. New, more planar substrates are therefore being
401 investigated to address this problem.

402 ■ CONCLUSION

403 In this work, a robust GNR film was integrated onto a flexible
404 polymer substrate, and its application as a radome deicer was
405 evaluated. On the basis of the RF transmission test (from 2.4 to
406 3.8 GHz) and simulations, the transmission loss was ultralow
407 and did not exceed 0.5 dB for any frequency below 3.8 GHz for
408 a GNR film with a thickness of 75 nm and did not exceed 1 dB
409 for a film with a thickness of 110 nm. The antenna range tests
410 showed that the measured transmission loss was in the range of
411 0.2–0.4 dB for any polarization in the angular sector ±60°. No
412 depolarization effect was detected. The deicing capability of the
413 GNR films was evaluated at –20 °C, and the efficient removal
414 of an ice coating under those cold conditions was
415 demonstrated. To the best of our knowledge, there is no
416 existing design of a deicing system that can provide such a RF-
417 transparent performance combined with low-weight, low-cost
418 materials. This underscores the efficacy of the GNR-based
419 nanomaterial for a performance unattained by conventional
420 materials.

421 ■ ASSOCIATED CONTENT

422 ● Supporting Information

423 Detailed derivation of an electromagnetic field through a thin
424 GNR film, high-resolution TEM images of GNRs, images of
425 GNR films on polyurethane-coated polyimide substrates,
426 experimental setup for measuring the resistance of the GNR
427 film under different temperatures, description of the deicing
428 video, details of the deicing test under –20 °C conditions,
429 HFSS infinite GNR film model, and dc sheet resistance versus
430 RF sheet resistance. This material is available free of charge via
431 the Internet at <http://pubs.acs.org>.

432 ■ AUTHOR INFORMATION

433 Corresponding Authors

434 *E-mail: vlad.vlad@verizon.net.

435 *E-mail: tour@rice.edu.

436 Author Contributions

437 ‡These authors have contributed equally

438 Notes

439 The authors declare the following competing financial
440 interest(s): Y.Z., V.V., and J.M.T. are coinventors on patent
441 applications (US201220808A1 and WO2012100178A1) owned
442 by Rice University and Lockheed Martin Corp. that disclose the
443 use of RF-transparent GNR films for radome deicing circuits.

444 ■ ACKNOWLEDGMENTS

The Lockheed Martin Corp. through the LANCER IV Program
445 provided funding, fabrication, and testing support. The AFOSR
446 (Grant FA9550-09-1-0581), the AFOSR MURI (Grant
447 FA9550-12-1-0035), and the ONR MURI Graphene Program
448 (No. 00006766, N00014-09-1-1066) provided funding for
449 GNR development. 450

451 ■ REFERENCES

- (1) Harris, D. C. *Materials for Infrared Windows and Domes: Properties and Performance*; SPIE Press: Bellingham, WA, 1999; p 80. 452
 - (2) Walton, J. D. *Am. Ceram. Soc. Bull.* **1974**, *53*, 255–258. 453
 - (3) Kirby, K. W.; Jankiewicz, A.; Kupp, D.; Walls, C.; Janney, M. *Mater. Technol.* **2001**, *16*, 187–190. 454
 - (4) Ramo, S.; Whinnery, J. R.; Van Duzer, T. *Fields and Waves in Communications Electronics*; John Wiley & Sons: New York, 1994; pp 455
 - (5) Novoselov, K. S.; Geim, A. K.; Morozov, S. V.; Jiang, D.; Zhang, 456
 - (6) Novoselov, K. S.; Geim, A. K.; Morozov, S. V.; Jiang, D.; 463
 - (7) Geim, A. K. *Science* **2009**, *324*, 1530–1534. 464
 - (8) Li, X.; Cai, W.; An, J.; Kim, S.; Nah, J.; Yang, D.; Piner, R.; 465
 - (9) Sun, Z.; Yan, Z.; Yao, J.; Beitler, E.; Zhu, Y.; Tour, J. M. *Nature* 466
 - (10) Jordan, E. *Electromagnetic Waves and Radiating Systems*; Prentice 467
 - (11) Genorio, B.; Lu, W.; Dimiev, A. M.; Zhu, Y.; Raji, A.-R. O.; 468
 - (12) Kosynkin, D. V.; Lu, W.; Sinitskii, A.; Pera, G.; Sun, Z.; Tour, J. 469
 - (13) Lu, W.; Ruan, G.; Genorio, G.; Zhu, Y.; Novosel, B.; Peng, G.; 470
 - (14) Zhu, Y.; Lu, W.; Sun, Z.; Kosynkin, D. V.; Yao, J.; Tour, J. M. 471
 - (15) Xiang, C.; Lu, W.; Zhu, Y.; Sun, Z.; Yan, Z.; Hwang, C.-C.; 472
 - (16) Thorp, J. S. *Proc. Inst. Electr. Eng., Part 3* **1954**, *101*, 357–359. 473
 - (17) Rouhi, N.; Jain, D.; Capdevila, S.; Jofre, L.; Brown, E.; Burke, P. 474
- J. Broadband Conductivity of Graphene from DC to THz. In *Proceedings of* 475
the IEEE International Conference on Nanotechnology, Portland, OR, 476
Aug 15–18, 2011; IEEE: Piscataway, NJ, 2011; pp 1205–1207. 477